Articles

Preparation and Characterizatin of MgO doped Fe_2O_3 Semiconductive Electrodes for Water Photodissociation

Il Kwang Kim*, Gabor A. Somorjai*, and Youn Geun Kim

Department of Chemistry, WonKwang University, Iri City 570-749
**Lawrence Berkeley Lab., Univ. of California, Berkeley, CA. 94720 USA.*

The preparation and characterization of semiconductive electrodes of MgO doped Fe_2O_3 were investigated. Pellets of MgO doped Fe_2O_3 were sintered at high temperatures between 1300℃ and 1400℃ and quenched rapidly in distilled water. The surfaces were analyzed by X-ray diffraction and scanning Auger electron spectroscopy. The surfaces of pellets contained both corundum structure (Fe_2O_3) and spinel structure ($Mg_xFe_{3-x}O_4$). Electrodes made of this material gave comparable anodic and cathodic photocurrents under illumination. The cathodic and anodic photocurrent on these photoelectrodes were verified high at 5-10 wt. percent that is critical doping amounts.

Introduction

Over the last ten years, iron oxide (α-Fe_2O_3) has been received considerable attention for possible application in photoelectrochemical cells for the dissociation of water because iron oxide has many desirable qualities[1,2]. This compound has a relatively small band gap, 2.1-2.3 eV that permits the use of about 40 percent of the solar photon flux incident on the earth's surface.[3] It is abundant and therefore inexpensive and it is stable in various aqueous solutions over a broad pH range. However, an external potential is needed in addition to illumination when using pure α-Fe_2O_3 to produce hydrogen and oxygen from water. Various ways to eliminate the need for using an external potential have been explored[4-7]. Recently, Gardner *et al.*[8] have reported that *p*-type (cathodic) photocurrents were generated from Mg doped Fe_2O_3 when the electrodes were sintered at high temperature. This cathodic photocurrent response was belived to be indicative of hydrogen production. It was suggested that this *p*-type behavior was due to vacancies introduced by substitution of Mg^{2+} into the iron (III) oxide matrix. Somorjai *et al.*[9,10] have obtained that the *p*-type semiconductors similar to the above produced hydrogen and photocurrent by photodissociation of water when illuminated on the surface of *p/n* diode in aqueous solution. However, the rate of hydrogen formation and quantum efficiency were extremely small.

The purpose of this work is to characterize these Mg doped iron oxide electrodes and their photoelectrochemical properties, and to understand on a fundamental level the source of these photocathodic currents. Photosemiconductor electrode was prepared with pellets of poly crystalline which sintered Fe_2O_3 doped with MgO. Furthermore, surface of the photoelectrode was characterized by X-ray diffraction and scanning Auger spectroscopy and its electrochemical properties were investigated by capacitance measurement and cyclic voltammetry.

Experiment

Preparation of MgO doped Fe_2O_3 photosemiconductive electrode. Mixed powders of Fe_2O_3 (MCB Chemists, reagent grade) and MgO (Mallinckrodt, analytical reagent grade) were weighed to give compositions between 0.1 wt. percent and 20 wt. percent. Pellets were then prepared using from 0.3 to 0.7 g of the homogeneous mixture which was pressed in 1/2 inch steel die at pressures between 8,000 and 9,000 kg/cm^2. The pellets were sintered in a platinum crucible for 20 hours at temperature between 1300 and 1400 ℃ in an electric furnace (Honeywell DCP-7). After sintering at these temperature, the disks were quenched in distilled water immediately. To each pellet, a kanthal wire was attached with silver epoxy (Tra-Con, Bipax) and insulated all the surface, except the surface exposed to the radiation, from solution using a silicon rubber (Dow Corning, Silastic 732 RTV sealant).

Characterization Techniques. X-ray diffraction patterns were recorded using a Siemens model D500 equipped with monochromated CuK_α radiation. All samples examined were thoroughly ground, then mounted on a lucite plate with silicon grease to avoid problems of preferred orientation. Diffractograms were recorded at a scan rate 3° 2θ/minute in the region $20° \leq 2\theta \leq 80°$ and phases were identified with the aid of ASTM card files.

The electrode surfaces were studied X-ray photoelectron spectroscopically using scanning Auger electron spectroscopy (Physical Electronics, Model 595 Multiprobe) which is equipped with X-ray source of MgK_α radiation and double pass cylindrical mirror analyzer.

Voltammograms were recorded using a potentiostat (Pine RDE-3) in a standard three electrode configuration with a Pt counter electrode and a saturated calomel reference electrode in a quartz cell. DC photocurrents were measured by illuminating the sample with filtered a 300 W tungsten-halogen lamp through water to reduce infrared radiation. This gave a average illumination intensity of approximately 300 mW/cm^2 as determined with a calibrated thermopile (Epply). AC photocurrents and capacitance were detected using a potentiostat (Pine RDE-3) and lock-in amplifier (PAR model 124 A) with a preamplifier in the differential mode.

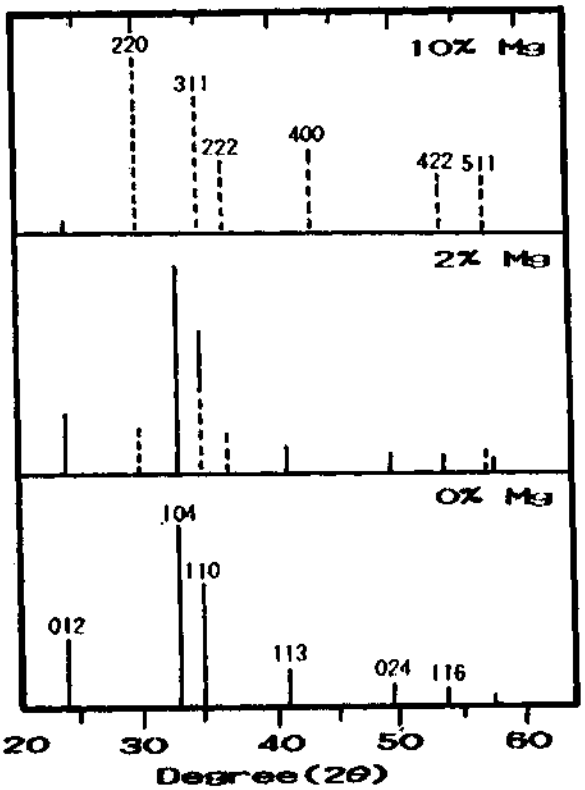

Figure 1. Typical X-ray diffraction patterns (CuK_α) for MgO doped Fe_2O_3 disks, ——; full solid line means a corundum phase; ·····; dotted line means a spinel phase.

Table 1. Characterization of Mg-doped α-Fe_2O_3 Samples

Sample No.	Mg (Wt.%)	Resistivity* (Ωcm)	Carrier Type	$\frac{I_{spinel}}{(I_{spinel}+I_{corundum})}$
1	0	10^6	n	0.0
2	2	3600	n,p	0.37
3	5	4	n,p	0.55
4	10	0.03	n,p	0.95–1.0

*Electrical properties of samples were measured using the Van der Pauw[11] four probe technique. Contacts to the samples were made using an silver epoxy and the ohmicity of the contact was verified by repetitive measurement of the resistivity at several different current magnitudes between 10 μA and 100 mA.

Results and Discussions

Surface Characteristics. X-ray diffraction patterns of powderic form sintered pellets showed the presence of hexagonal corundum (Fe_2O_3) and cubic spinel phases (Fe_3O_4 or $MgFe_2O_4$). Figure 1 shows that the amount of spinel phase found in these pellets depends mainly on the concentration of magnesium oxide. We have prepared samples with different ratios of corundum and spinel phases, in order to study the relationship between the spinel phase concentration and the intensity of photocurrents.

Characteristics of these samples including the Mg dopant levels, resistivity, and measured carrier type are summarized in Table 1. The room temperature resistivity of these iron oxides varies from 10^6 Ω cm for the pure α-Fe_2O_3 phase (sample 1) to 0.03 cm for the sample with the richest concentration of the spinel phase (sample 4). Table 1 presents the uncorrected integrated intensity ratio of the spinel (220) reflection to the (012) Fe_2O_3 corundum reflection. This ratio is an indication of the relative concentration of spinel in the ceramic disc. It is evidence that the addition of magnesium to the iron oxide enchances the formation of the spinel phase.

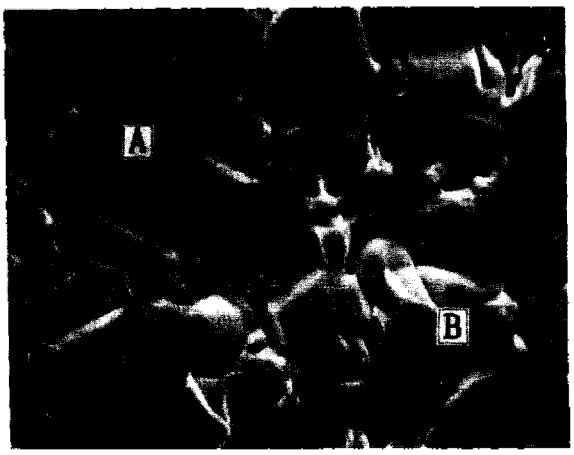

Figure 2. A typical SEM photograph of 8.0% MgO-Fe_2O_3. A: $Mg_xFe_{3-x}O_4$ B: α-Fe_2O_3

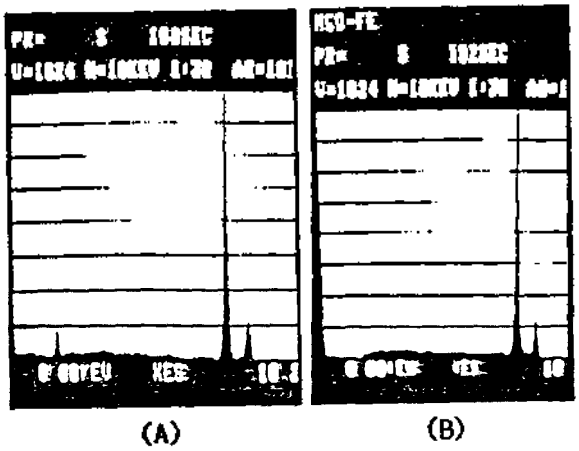

Figure 3. X-ray photoelectron spectra of 8.0% MgO doped Fe_2O_3 disk.

Surface Analysis. Scanning electron micrograph shown in Figure 2 depicts the surface topography of Fe_2O_3 pellet doped with 8.0 wt. percent MgO. The surface appeared to co-exist as polycrystalline having two kind of structures. In order to determine the composition of magnesium in the corundum lattice, we have performed elemental analysis on the selected regions of polycrystalline surface, and the results are shown in Figure 3.

Kuczynski[12] has investigated the mechanism of the formation of $MgFe_2O_4$ from the binary oxides and suggested that the formation of the spinel occurs by diffusion of cations across grain boundaries. At high temperatures, oxygen is lost from Fe_2O_3 and exchange of Fe^{2+} and Mg^{2+} can occur by diffusion, resulting in spinel phase. In the present case,

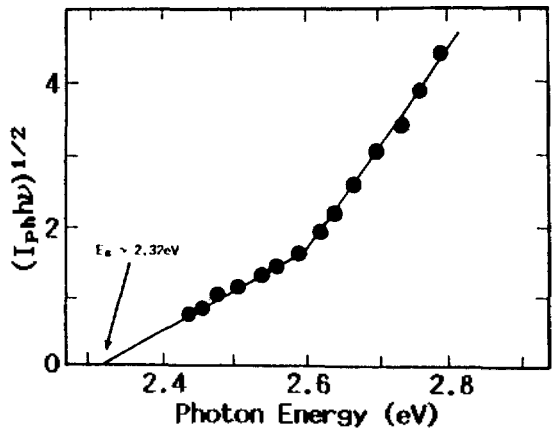

Figure 4. Band gap determination of 8.0% MgO doped Fe_2O_3 electrodes from photocurrent dependence on wavelength.

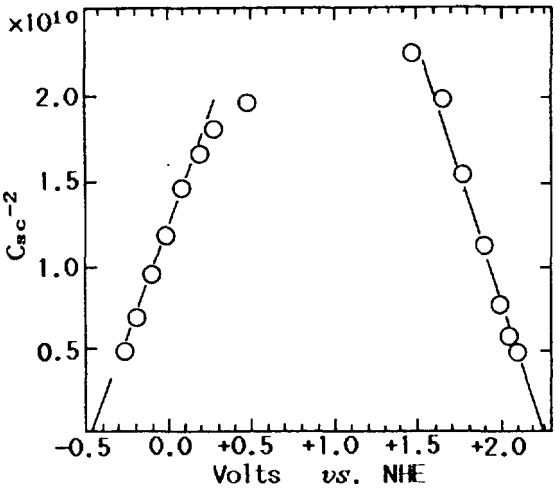

Figure 5. Mott-Schottky plots on the inverse square of space charge capacitance *vs.* applied potential for 8.0% MgO doped Fe_2O_3 electrode.

it is likely that even in the initial spinel, $MgFe_2O_4$, further cation exchange takes place so that the solid solution $Fe_{3-x}Mg_xO_4$ is formed. This would explain the large amounts of spinel formed at temperatures below the corundum-spinel transition temperature of Fe_2O_3 in mixtures containing only a small amount of magnesium oxide. (10% or less).

Measurement of Band Gap Energy. Next, we determined the band gap and the transition mode of the MgO doped Fe_2O_3 pellets using the following relationship[13,14].

$$I_{ph}=A\frac{(h\nu-E_g)^{n/2}}{h\nu}$$

where I_{ph} is the photocurrent, $h\nu$ is the energy of illumination, E_g is the band gap energy, A is a constant depending on the applied potential, and n depends on whether the bandgap transition is direct ($n=1$) or indirect ($n=4$). Following this equation, we plotted $(I_{ph}\ h\nu)^{1/2}$ versus $h\nu$ using the photocurrent spectrum, and the result is shown in Figure 4.

The linear fit with $n=4$ confirms that the MgO-doped Fe_2O_3 pellet is an indirect bandgap semiconductor. The intercept of the photon energy axis yields a band gap of 2.32 eV in agreement with published values for the bandgap of undoped and doped Fe_2O_3[15,16].

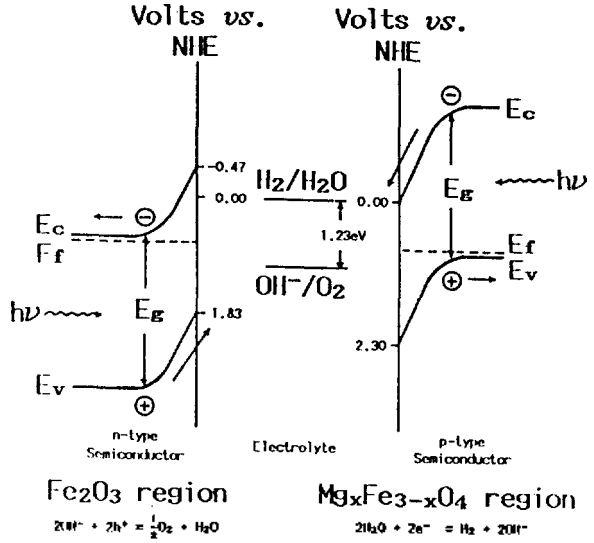

Figure 6. Energy level diagram for depicting band edge locations of 8.0% MgO doped Fe_2O_3 relative to hydrogen/oxygen redox couples.

Therefore, the photon energy should be over 2.30 eV which could increase the photocurrent and hasten the activation of hydrogen formation in MgO doped Fe_2O_3 system.

Capacitance Measurements. The locations of conduction and valence band edges with respect to redox couples in solution are of citical importance. To determine the location of these edges on the electrochemical scale, Mott Schottky[13] measurements that the capacitance of the space charge layer was performed for MgO doped Fe_2O_3 electrodes according to Horowitz[17] method using a phase shift technique. In Figure 5, we ploted the inverse square space charge capacitance ($1/C_{sc}^2$) versus applied potential to obtain the flat-band potential from the intercept for *n*-type or *p*-type surface.

We have obtained flat-band potentials which have both conduction band edge ($E_c=-0.47$ volts *vs.* NHE) and valence band edge ($E_v=+2.30$ volts *vs.* NHE) as compared with Calvin[18] and Goodenough[19] acquired only conduction band edge ($E_c=-0.50$ volts *vs.* NHE) of n-type electrode. We have determined band edges from Mott Schottky plots as descried above and extrapolated using the measured band gap (2.3 eV) to find the alternate band edges. Informations on flat-band potentials can therefore be used to generate an energy level diagram as shown in Figure 6. This shows the interfaces between the electrolyte and the *n*-type or *p*-type surfaces. From this diagram, one can easily see how the *p/n* assembly operates. Upon illumination in solution, electron hole pairs are produced in MgO-doped Fe_2O_3 electrodes. In the *p*-type region, electrons are driven through the depletion layer towards the interface where they convert hydronium ions in solution to hydrogen. Conversely, vacancies driven to the *n*-type region convert hydroxyl species to oxygen. In both regions, the majority carriers migrate away from the surface to produce the observed photocurrents. Thus hydrogen evolution occurs at the *p*-type region and oxygen evolution takes place at the *n*-type region.

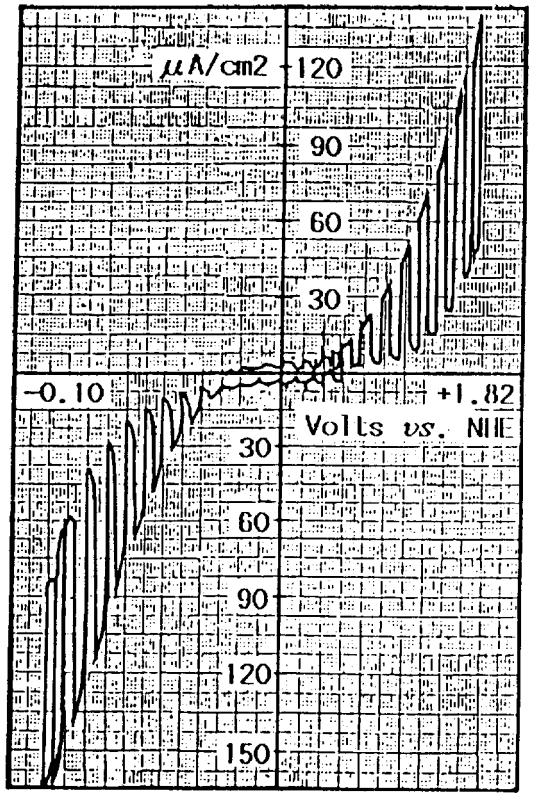

Figure 7. Cyclovoltammetric photocurrents for the 8.0% MgO doped Fe_2O_3 electrode at pH=13.

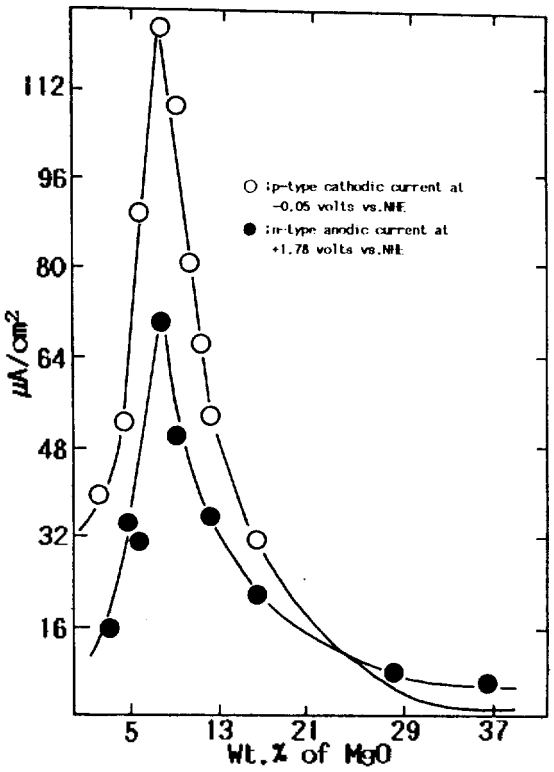

Figure 8. Photocurrent depend on the doping amount of MgO.

Photoelectrochemical Measurements. Figure 7 is a typical D.C. cyclic voltammogram in 0.1 M NaOH of an electrode having a composition of 8.0 wt. percent MgO in Fe_2O_3. The electrodes of these material exhibit dual properties of anodic and cathodic photocurrent that are characteristic of *n*-type and *p*-type photosemiconductors as a result of inhomogeneties in the near surface region. The dark currents observed between −0.02 and +1.73 volts *vs.* NHE are on the order of 60 μA/cm². The dark currents of these materials evolves with time, reaching values as high as 80 μA/cm². It means that the electrode may not be stable under cyclic voltammetric conditions. Under illumination the electrodes exhibit both cathodic and anodic photo-current which have initial values of up to 80 μA/cm² at −0.02 volts *vs.* NHE and 60 μA/cm² at +1.73 volts *vs.* NHE.

Several electrodes were prepared and studied under identical conditions except that the weight percent of magnesium (Mg/Mg⁺ Fe) was altered between 1.0 and 35.0 percent. Photocurrent densities measured in 0.1 M NaOH solution are shown in Figure 8. We confirmed that anodic photocurrent and cathodic photocurrent are remarkably increased in the samples of 5.0 to 8.0 wt. percent doped MgO.

Conclusion

The preparation and characteristics of magnesium substituted iron oxide ceramics have been examined. It was found that the sintering of cold pressed disks made from MgO and Fe_2O_3 powders at temperatures between 1300 and 1400℃ resulted in heterogeneous ceramic material containing both α-Fe_2O_3 and a spinel phase, most likely of composition $Fe_{3-x}Mg_xO_4$. Capacitance and photoelectrochemical measurements showed that this electrodes prepared from the sintered disks exhibited dual properties of *n*-type and *p*-type photosemiconductor.

These results motivated a model for photocurrents response in the MgO-doped iron oxides, which involved the presence of two phases, a bulk corundum (α-Fe_2O_3) and surface spinel phase ($Fe_{3-x}Mg_xO_4$). It is proposed that a gradient is formed at the interface between these two phases due to mismatched electrochemical potentials. While this model is consistent with all characterizations performed on these electrodes, hydrogen evolution does not correlate with observed photocurrent when these materials are illuminated in aqueous solution. It seems that a substantial portion of the observed DC photocurrents is due to a photoreduction of oxygen dissolved in solution. Therefore, it seems likely that the hydrogen is produced instead by a local photosynthetic process which does not require transport of carriers through the electrode bulk surface. Studies are in progress to elucidate to details of hydrogen production in this system.

References

1. J. H. Kennedy, R. Shinar and J. P. Ziegler, *J. Electrochem. Soc.*, **127**(10), 2307 (1980).
2. H.L. Sanchez, H. Steinfink and H. S. White, *J. Solid State Chem.*, **41**, 90 (1982).
3. L. A. Marasak, R. Messier and W. B. White, *J. Phys. Chem. Solids*, **41**, 981 (1980).
4. D. S. Ginley and M. A. Butler, *J. Appl. Phys.*, **48**, 2019 (1977).

5. R. Shinar and J.H. Kennedy, *Solar Energy Mat.*, **1**, 237 (1979).
6. I. T. Liou, C. Y. Yang and S. N. Levine, *J. Electrochem. Soc.*, **129**, 342 (1982).
7. H. Yoneyama, H. Sakamoto and H. Tamura, *Electrochem. Acta* **20**, 341 (1975).
8. R. F. Gardner, F. Sweett and D. W. Tanner, *J. Phys. Chem. Solids*, **24**, 1183 (1963).
9. C. H. Leygraf, M. Hendewerk, G. A. Somorjai, *J. Catal.*, **78**, 341 (1982).
10. J. E. Turner, M. Hendewerk, G. A. Somorjai, *J. Electrochem. Soc.*, **131**, 1779 (1984).
11. L. J. Van der Pauw, *Phillips, Res. Rep.*, **13**, 9 (1958).
12. G. C. Kuczynski, "Ferrites" Pro. of the International Conference, p. 87-95, University Park Press, Baltimore, MD (1971).
13. M. A. Butler, *J. Appl. Phys.*, **48**, 1914 (1977).
14. M. A. Butler, D. S. Ginley, M. Eibschultz, *J. Appl. Phys.*, **48**, 3070 (1977).
15. A. Heller, W. A. Bonner, *J. Electrochem. Soc.*, **129**, 1701 (1982).
16. A. Heller, D. E. Aspres, *J. Phys. Chem.*, **87**, 4919 (1983).
17. G. Horowitz, *J. Electroanal. Chem.*, **159**, 421 (1983).
18. M. Calvin, K.G. McGreger, J. W. Otovos, *J. Appl. Phys.* **50**, 369 (1979).
19. J.B. Goodenough, M. P. Dare-Edwards, *J. Chem. Soc., Faraday Trans.*, **79**, 2027 (1983).

FT-IR Studies of Molybdena Supported on Titania

Kwan Kim* and Soon-Bo Lee+

Department of Chemistry, Seoul National University, Seoul 151-742
+Department of Chemistry, Sung Kyun Kwan University, Suwon 440-746
Received May 28, 1990

Fourier transform infrared spectroscopy has been applied to the characterization of titania supported molybdena. The equilibrium adsorption method seemed to produce molybdena species homogeneously dispersed on the support. Even under an oxidizing environment, molybdena species appeared to be able to possess coordinatively unsaturated Mo^{5+} ions owing to the natures of TiO_2, i.e. oxygen deficiency and permeability toward oxygen diffusion. At the initial stage of reduction, the terminal double bond oxygen (Mo=O) seemed to be removed, generating presumably Mo^{4+}. The carbonyl bands at 2198 and 2190 cm^{-1} observed after CO exposure were attributed to the $Mo^{5+}\cdots CO$ and $Mo^{4+}\cdots CO$ complexes, respectively, while the band pair at 2136 and 2076 cm^{-1} to $Mo^{4+}(CO)_2$.

Introduction

There is considerable current interest in the strong interaction between certain oxide support and metal phase (SMSI)[1-3]. In addition, the interaction between oxide supports and highly dispersed oxide phases is receiving increasing attention[4-7].

Supported oxides of transition metals of group VIb (Cr, Mo, W) are widely used as catalysts for various reactions. For example, alumina-supported molybdenum based catalysts are extensively used in the hydrotreating processes such as hydrodesulfurization, hydrodenitrogenation and hydrodemetalization of petroleum or coal products[8-12]. The oxidation of hydrocarbons, carbon monoxide hydrogenation and water gas shift reaction are also catalyzed by supported molybdena. Reviews and useful discussions of various aspects of the alumina supported molybdena catalyst have been published[8-12], but conclusions tend to be controversial and contradictory. The confusion is attributable, in part, to the variety of catalysts studies and to differences in preparation and/or pretreatment of catalysts of similar composition.

Titania is a typical SMSI oxide. SMSI is characterized by the loss of a supported metal's ability to chemisorb CO or H_2 following high temperature reduction[1]. Early explanations of the SMSI effect centered on an electronic model wherein the chemical properties of metal were altered via a charge transfer between the support and the metal[2]. More recently, there is a growing body of evidence that a reduced form of titania migrates onto the metal surface during high temperature reduction[3]. The origin of chemisorption suppression is explained in terms of a simple loss in surface adsorption sites. The detailed mechanism of TiO_x-overlayer formation, occurring within minutes at moderate temperatures[13] is still obscure, however[3].

Based on the above description, one may expect that titania would modify the surface state of the supported molybdena. In fact, Segawa *et al*[14]. reported that titania supported molybdena catalyst exhibited two types of active sites after reduction: one site was active for hydrogenation, and the other site was active either for isomerization or metathesis.

Many spectroscopic techniques have been applied to the study of molybdena/titania catalysts, including ESCA[15,16], ISS[17] and laser Raman[17,18]. These methods, however, do not yield information on specifically those surface atoms which are "exposed" or "coordinatively unsaturated" (cus), among which, presumably, are to be found the sites active for catalysis.

Among the spectroscopic techniques most useful for sur-